# Development of a Castering Nosegear for a Tandem Wing Light Aircraft

Imraan Faruque

imraan@umd.edu

*Department of Aerospace Engineering, University of Maryland,*

*3182 Glenn L Martin Hall*

*College Park, MD, 20742, USA*

**Tandem wing aircraft can provide induced drag savings and additional control strategies. However, the forward CG location and higher landing speeds make design of the nose gear particularly important to operational success. This paper presents structural, dimensional, and shimmy-avoidance studies for a light tandem wing aircraft model with identical sized wings and a history of nosegear malfunctions. An example of the gear design is fabricated and load tested during typical landing loads. The structural analysis shows that the limit loads are determined by bending moment stresses near the firewall mount and in the forward tubing bend during landings, and that fatigue margins are ample. The gear test includes experimental IMU data from several points on the fuselage and places them in the context of linear elastic energy equivalence and finite element analysis results.**

## I. Introduction and Background

Tandem wing aircraft configurations have shown promise as unmanned aerial system platforms, due to the potential for induced drag savings at reduced wingspans, and the relaxation of the underactuation constraint found in many aerospace vehicles. Initial work on tandem wing aircraft began on manned aircraft and grew out of a desire to reduce induced drag [7, 6, 8], soon identifying the role of CG location in the choice of 2 and 3 wing configurations. More recent work has focused on small tandem wing aircraft used as unmanned aerial vehicles. The tandem wing configuration has particular relevance for the application of morphing wing results such as Cusher and Gopalarathnam [2], as the provision of flaps on two equally-sized lifting surfaces allows dynamic control of longitudinal lift distribution and enhanced control over aerodynamic forces during CG movements. The interest in tandem wing UAVs has also led to more general morphing tandem wing applications at other scales [13]. However, tandem wing aircraft have differing center of gravity locations, which has ramifications for the nosewheel design, and a standard nosegear may not be appropriate. In some cases, designers have even mitigated the landing gear design issue via VTOL concepts [11, 12].

The aircraft example selected for this study is the Quickie Tri-Q200 aircraft, shown in Fig 1, which is powered by a Continental 0-200 engine and has two identically-sized wings. This aircraft was initially designed with a conventional gear arrangement, but conversion to tricycle gear has been attempted successfully several times. While accidents associated with unmanned aerial systems (UAS) are not recorded, the US National Transportation Safety Board and the UK Air Accident Investigation Branch do record manned aircraft accidents, indicating a total of 11 accidents associated with the model, of which 4 include mention of nosegear collapse. Given the differing loading configurations, is it possible that a more detailed academic analysis of the structural and dynamic properties of a nosegear could inform our understanding of the nosegear conversion?

This paper presents design studies for a replacement nosegear used on a Q200 tandem wing flight dynamics platform to place the tailwheel to nosewheel conversion in context, and reports on load testing done after fabrication and assembly of an example gear.

**Figure 1. Example tandem wing aircraft, a Tri-Q200.**

## II. Design Studies

This section presents design studies, including loads analysis, structural modeling, and shimmy avoidance criteria.

### A. Structural Analysis

#### 1. *Loads*

Operating loads on the nosegear were computed from weight and balance loading configurations in the most extreme loading configuration. Braking loads were included via computation of the maximum nosegear dynamic load $W_{n,m}$

$$W_{n,m} = W(F - L)/F + \frac{aJW}{gF}, \tag{1}$$

where $W$ is the maximum gross of weight the vehicle, $a$ the braking deceleration, and the other quantities defined in Fig 2(a) [1]. Figure 2(b) shows the effect of including the additional braking loads, indicating the linear relation of braking loads with respect to CG height.

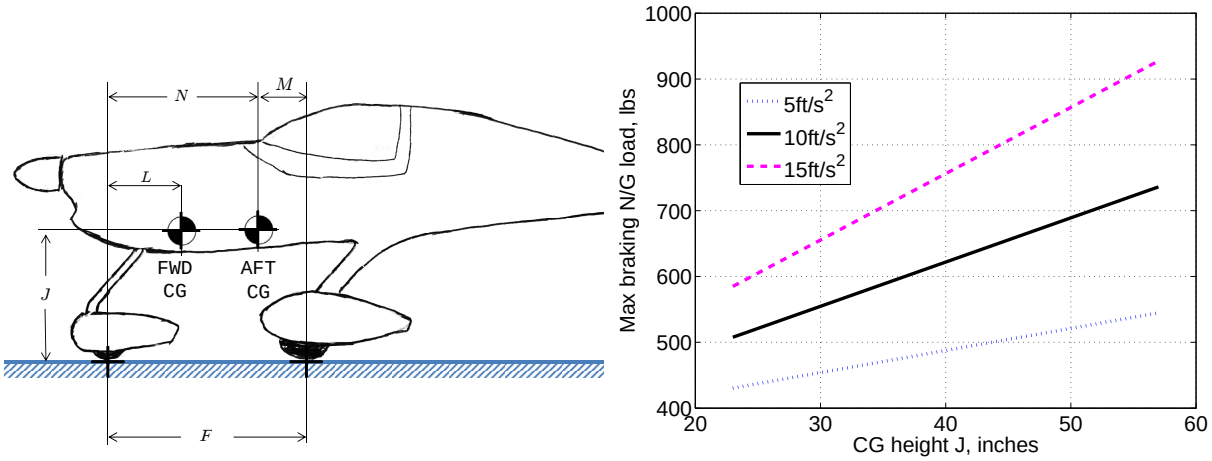


**Figure 2. Nosegear dynamic loading under braking conditions at maximum gross weight.**

A finite element model of the geometry was created to allow for detailed stress and deformation values under these loading configurations to be compared against experimental results. Due to differences in installations and the complexity of composite airframe deformation, two cases were modeled: (a) the forward mount rigidly constrained and aft mount unsecured, (b) both forward and aft mounts rigidly constrained. In both cases, the tire and fork assembly was considered rigid and a vertical load was applied to the tire

contact patch. Material properties used were AISI 4130 Steel, water quenched 855C (1570F), 480C (900F) temper, 13mm (0.5 in.) round, Rockwell C 36 [9].

### 2. *Fatigue*

Fatigue failure in steel structures is uncommon because steel has no endurance limit, but was addressed here because one accident report contained a report of possible fatigue. To address the effect of surface imperfections on repeated loadings during taxiing, stress levels in the part were compared against allowable stresses $\sigma_a$, which is fatigue stress limit $\sigma_s$ derated for static mean stress $\sigma_m$ via the Goodman relation,

$$\sigma_a = \sigma_f \left(1 - \frac{\sigma_m}{\sigma_{ts}}\right), \tag{2}$$

where $\sigma_{ts}$ is the ultimate tensile strength of the material. The effect of mean stress is shown in Fig 3, which also indicates the design operating point of 35 ksi. Allowable stress is 50 ksi, indicating that fatigue margins are ample.

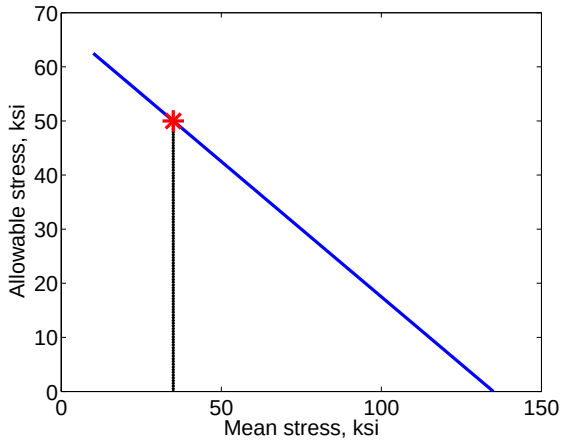


**Figure 3. Allowable stress for AISI 4130 Heat treated, showing design operating point of 35 ksi.**

## B. Dimensional Requirements

### 1. *Fit and Clearance*

Lifting surface performance during takeoff and landing roll specified a front wing ground incidence of 3-5° in all configurations. Federal Aviation Regulations Part 23.925(a)'s requirement of a minimum 7 in propeller ground clearance did not further constrain the ground incidence height.

### 2. *Shimmy Avoidance*

Shimmy is a complex nonlinear phenomenon involving complex dynamic modeling including configuration [10], tire inflation and elasticity, gyroscopic coupling, and bearing tolerances [3], which is beyond the scope of this presentation. Instead, a lower bound on spindle friction that will prevent shimmy was computed. Previous work [5] has developed experimental and theoretical models of kinematic shimmy, which may be solved to find a closed form expression for the spindle friction $T$ that will prevent kinematic shimmy for certain castering configurations

$$T = 0.17\mu R W_n, \tag{3}$$

in terms of tire-to-concrete coefficient of friction $\mu \equiv 0.55$, distance from pivot axis to wheel center $R$ (mechanical trail), and weight on the tire $W_n$. The resulting force of 16.3 lbs is higher than comparable aircraft such as the Diamond DA-20, which requires $9 \pm 1.25$lbs. Reduction of this specification may be justified after operational testing. Applicability of this mathematical model is to castering wheels with small positive caster angle, leading to an additional design requirement.

### C. Fabrication of Gear and Free Drop Test Rig

The nosegear gear strut was fabricated from annealed AISI 4130 steel. After welding, the welds were stress relieved and the part heat treated to a hardness of Rockwell C 42. Distortion throughout stress relief and heat treat stages was less than 0.010 in on all dimensions. The fork was fabricated from 6061 aluminum, and a brass bushing inserted with an interference fit. Epoxy-based zinc phosphate primer and topcoat was applied as a surface treatment to both components prior to test.

A test rig was established allowing the complete aircraft to be tested in free drop configuration, providing capability to provide drop heights in excess of the 9.2 to 18.7 in maximum drop height established in 14 CFR 23.725. Normal drop tests were conducted with a descent velocity of 2-3 ft/s as established in J A Hootman and A R Jones [4] as a normal landing. Aerodynamic effects were assumed negligible during the free drop to establish the drop $\Delta h$ as a function of desired descent velocity $V$ and gravitational acceleration $g$.

$$\Delta h = \frac{V^2}{2g}, \tag{4}$$

which specified a required drop height of 1.68 in.

Small MEMs-based inertial measurement units were calibrated and installed at the gear attachment location and fuselage forward CG location. The spring constant $k_x$ from the FEA results of Section A may be used to choose a drop height corresponding to a peak G loading $G_{\texttt{peak}}$ via energy equivalence between gravitational potential and linear elastic storage,

$$\Delta h = G_{\texttt{peak}}^2 \frac{mg}{2k_x}, \tag{5}$$

which is shown for both the aft slip piece fixed and free conditions in Fig. 4.

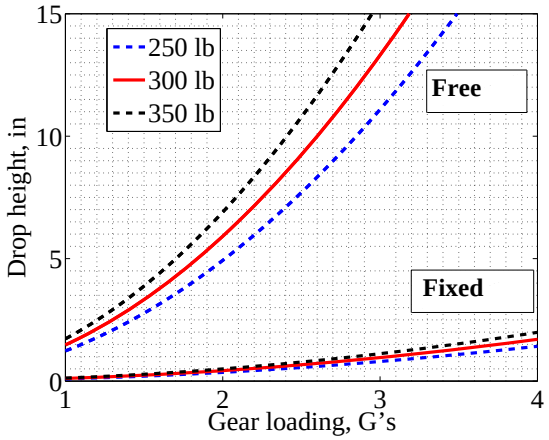


**Figure 4. Drop test height required for a given peak G load for both aft-fixed and aft-free load conditions and varying nosewheel loading.**

## III. Results

### A. Structural

| Loading Condition | Nosewheel weight | Nosegear Stress |
|---|---|---|
| Empty | 248 lb | 34.2 ksi |
| Gross | 248 lb | 34.2 ksi |
| Fwd | 271 lb | 37.4 ksi |

**Table 1. Peak Von Mises stress level in simplified FEA model is under the fatigue limit in all loading conditions**

A finite element modeling approach shows that changes in the mounting conditions of the aft mount cause significant changes in stress levels, as seen in Fig 6. An FEA analysis with the aft mount unsecured indicates that peak Von Mises stress in the component occurs adjacent to the weld junction between the plate and tubing at 2.561 MPa/lb (0.371 ksi/lb). Conversely, the with the aft mount secured, peak Von Mises stress is attained in the forward bend at 0.953 MPa/lb (0.138 ksi/lb). With the aft mount secured and in the most extreme loading configuration (forward loading), yield stress occurs at an overall aircraft 4.3G loading, versus plastic yield beginning at only a 1.6G load case when the aft mount is unsecured.

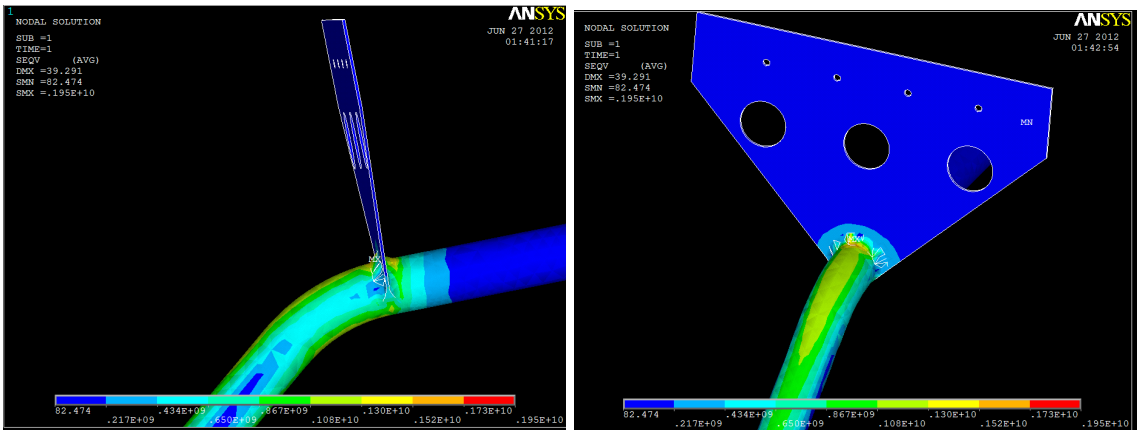


(a) Side View (b) Quarter View

**Figure 5. Peak stress occurs adjacent to the plate/tube weld junctions when aft mount is free.**

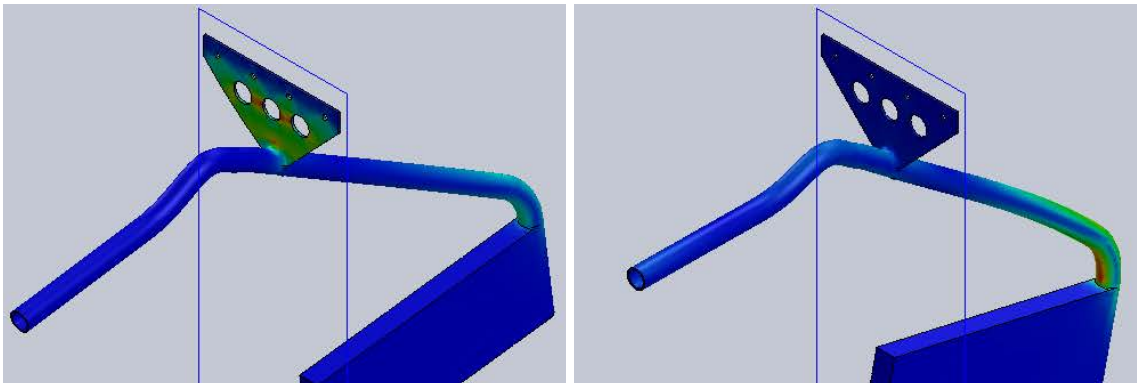

(a) Aft Mount Unsecured (b) Aft Mount Secured

**Figure 6. Changes in mounting configuration change the magnitude and location of peak stress.**

## B. Load Testing Results

To simulate a normal landing load configuration, the installed gear was tested with drop heights varying from 0 (tire crush only) to 3.25 inches. Based on Eqn (4), descent velocities were up to 4.2 ft/s. Telemetry was recorded from the installed accelerometers at 100 Hz, with expected peak velocities given by Eqn (5). Data for two of the tests are shown in Fig 7, from which a natural frequency of 4.07 Hz may be computed. The recorded test data also makes clear the effect of not including damping. While the vehicle experiences aerodynamic damping during landing, integrating an oleo or elastomeric unit could be a possible improvement to reduce the number of oscillations.

The peak vertical accelerations recorded in the test are shown in Fig 8 along with the theoretical fixed and free tailpiece boundaries from Section C. Tire elastic effects are visible as the 1.5G recorded load at 0 in

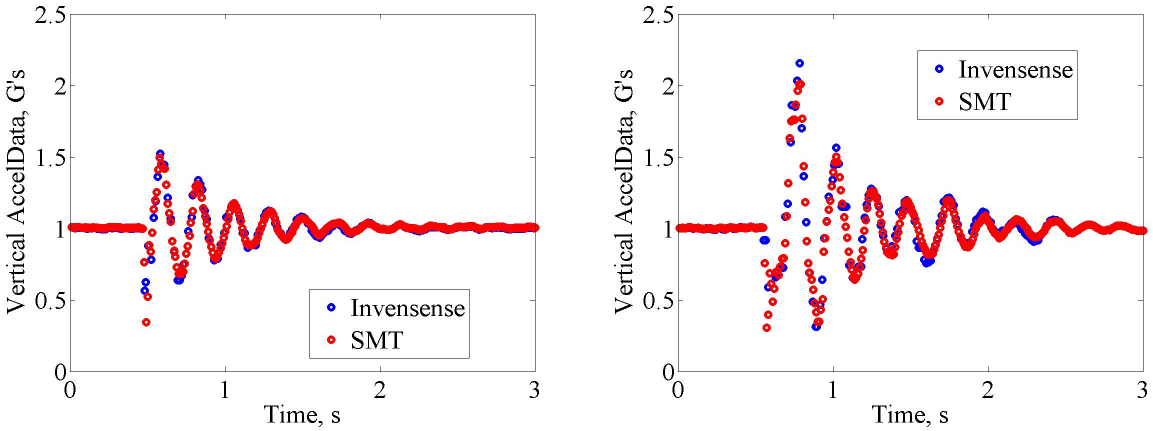


(a) 0.0 in (b) 2.25 in

**Figure 7. Vertical accelerations recorded on firewall (Invensense) and on fuselage (SMT).**

drop height, but the other drop height data is contained within the theoretical boundaries of fixed and free aft mounts.

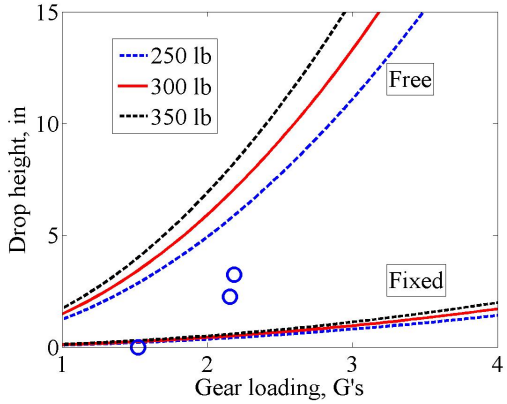


**Figure 8. Peak recorded vertical accelerations and theoretical boundaries.**

## IV. Conclusions

This study described theoretical, computational, and experimental analysis of a castering nosegear commonly installed on a tandem wing aircraft model. Theoretical conditions for shimmy avoidance were presented, requiring rotational drag equivalent to a 16.3 lb side force on the wheel axle. A finite element analysis was used as a structural model to quantify spring rates and estimate stress locations. The analysis indicates that fatigue margins are ample and that the proper constraints of the aft mount are important to the strength of the installed component, leading to significant differences in stiffness and stress level. The tubing/plate junction and the forward tubing bend are identified as the locations of peak stress. The nosegear was mechanically fabricated and installed, and instrumented with inertial measurement equipments to indicate the stress levels during the experimental test. The recorded inertial data indicated that the theoretical and computational upper and lower bounds bracketed the experimental results, and that the nosegear may benefit from integrating a damping mechanism to reduce oscillation.

## References


[1] Norman S Currey. *Aircraft Landing Gear Design: Principles and Practices*. AIAA Education Series, 1988.

[2] Aaron A Cusher and Ashok Gopalarathnam. Drag reduction on aircraft configurations with adaptive lifting surfaces. In *46th AIAA Aerospace Sciences Meeting and Exhibit*, Reno, Nevada, January 7-10 2008.

[3] Chris Howcroft, M Lowenberg, S Neild, and B Krauskopf. Effects of freeplay on dynamic stability of an aircraft main landing gear. *Journal of Aircraft*, 50(6):1908–1922, 2013.

[4] J A Hootman and A R Jones. Results of Landing Tests for Various Airplanes. Technical Report NACA-863, National Advisory Committee for Aeronautics, 1942.

[5] Arthur Kantrowitz. Stability of Castering Wheels for Aircraft Landing Gears. Technical Report NACA-686, National Advisory Committee for Aeronautics, 1940.

[6] Eric R Kendall. Performance Trades of Two-Surface and Three-Surface Configurations. In *General Aviation Technology Conference*, number 84-2221, Hampton, VA, July 10-12 1984.

[7] Eric R Kendall. The Aerodynamics of Three-Surface Airplanes. In *AIAA/AHS/ASEE Aircraft Design Systems and Operations Meeting*, number 84-2508, San Diego, CA, Oct 31-Nov 2 1984.

[8] Eric R Kendall. The Minimum Induced Drag, Longitudinal Trim and Static Longitudinal Stabiliity of Two-Surface and Three-Surface Airplanes. In *AIAA 2nd Applied Aerodynamics Conference*, number 84-2164, Seattle, WA, Aug 21-23 1984.

[9] MatWeb LLC. Matweb material property database, February 2014. URL `http://www.matweb.com/`.

[10] Ladislao Pazmany. *Landing Gear Design for Light Aircraft*. Pazmany Aircraft Corp, 1986.

[11] H Stone and KC Wong. Preliminary design of a tandem-wing tail-sitter UAV using multi-disciplinary design optimization. In *AUVSI Proceedings*, 1996.

[12] RH Stone. Modeling and control of a tandem-wing tail-sitter UAV. *Modeling and Control of Mini-Flying Machines*, 127, 2005.

[13] G Q Zhang and S C M Yu. Unsteady aerodynamics of a morphing tandem-wing unmanned aerial vehicle. 2012.